Nano Research
DOI 10.1007/s12274-016-1240-5
Research Article
ISSN 1998-0124
CN 11-5974/O4

Temperature dependence of pyro-phototronic effect on self-powered ZnO/perovskite heterostructured photodetectors

Wenbo Peng[1,2,§], Ruomeng Yu[1,§], Xingfu Wang[1,§], Zhaona Wang[1], Haiyang Zou[1], Yongning He[2], and Zhong Lin Wang[1,3] (✉)

[1] *School of Materials Science and Engineering, Georgia Institute of Technology, Atlanta, Georgia 30332-0245, USA*
[2] *School of Electronic and Information Engineering, Xi'an Jiaotong University, Xi'an 710049, China*
[3] *Beijing Institute of Nanoenergy and Nanosystems, Chinese Academy of Sciences, Beijing 100083, China*
[§] *These authors contributed equally to this work.*

Received: 14 June 2016
Revised: 26 July 2016
Accepted: 28 July 2016

KEYWORDS
self-powered,
ZnO,
perovskite,
pyro-phototronic effect,
temperature dependence

ABSTRACT

Self-powered ZnO/perovskite heterostructured ultraviolet (UV) photodetectors (PDs) based on the pyro-phototronic effect have been recently reported as a promising solution for energy-efficient, ultrafast-response, and high-performance UV PDs. In this study, the temperature dependence of the pyro-phototronic effect on the photo-sensing performance of self-powered ZnO/perovskite heterostructured PDs was investigated. The current responses of these PDs to UV light were enhanced by 174.1% at 77 K and 28.7% at 300 K owing to the improved pyro-phototronic effect at low temperatures. The fundamentals of the pyro-phototronic effect were thoroughly studied by analyzing the charge-transfer process and the time constant of the current response of the PDs upon UV illumination. This work presents in-depth understandings about the pyro-phototronic effect on the ZnO/perovskite heterostructure and provides guidance for the design and development of corresponding optoelectronics for ultrafast photo sensing, optothermal detection, and biocompatible optoelectronic probes.

1 Introduction

Because of its non-central symmetric crystal structures and unique physical properties, wurtzite-ZnO is one of the most widely used piezoelectric semiconductor materials for various electronic/optoelectronic applications, including energy-harvesting devices [1, 2], field-effect transistors [3, 4], logic circuits [5, 6], ultraviolet (UV) lasers and light-emitting diodes [7, 8]. In particular, ZnO-based UV photodetectors (PDs) have attracted tremendous attention in the past decade owing to their wide direct bandgap (3.3 eV) and high exciton binding energy (60 meV) at room temperature [9–12]. With the use of ZnO nanostructures as building

Address correspondence to zhong.wang@mse.gatech.edu

blocks, numerous UV PDs have been demonstrated [13–17], exhibiting a high photoresponsivity, sensitivity, and/or specific detectivity. However, the relatively long response time ranging from a few to hundreds of seconds inevitably hinders their practical applications [18–22]. Therefore, it is highly important to develop ZnO-based PDs with an ultrafast response time and competitive sensing performance.

A self-powered ZnO/perovskite heterostructured (ZPH) PD utilizing the UV light self-induced pyroelectric effect in ZnO to enhance the UV photosensing performance was previously demonstrated [23]. Upon UV illumination, transient temperature changes occur in ZnO and lead to the distribution of the pyroelectric polarization potential across the polar direction of the ZnO nanowire array because of the non-central symmetric crystal structure [24–26]. The charge-carrier transport processes and the photosensing performances of ZPH PDs are modified owing to these pyroelectric polarizations, which are known as the pyro-phototronic effect [23]. Moreover, the ZnO/perovskite heterostructure configuration enables unique self-powered UV sensing operations under zero bias based on the photovoltaic effect with a low dark current (<0.1 nA), a high responsivity, and ultrafast response times (tens of microseconds). Because the pyro-phototronic effect is fundamentally new in science and was not studied before ZPH PDs, it is essential to investigate its physical working mechanism systematically and carefully, not only for understanding the fundamentals of the separation and migration of charge carriers but also for guidance in designing and developing high-performance pyro-phototronic devices for optoelectronic applications.

In this work, the temperature dependence of the pyro-phototronic effect on ZPH PDs is systematically investigated by varying the temperature from 77 to 300 K under a series of UV illuminations at each temperature. The current-response improvement of the PDs due to the pyro-phototronic effect is significantly enhanced by over 500% as the system temperature decreases to 77 K, as the temperature change is relatively large compared with the initial temperature in ZnO upon UV illumination. By analyzing the photocurrent and calculating the effective charge transfer due to the pyroelectric polarizations at various temperatures, the fundamental working mechanism of the pyro-phototronic effect is carefully studied. In addition, the influences of bias voltages on the pyro-phototronic effect are investigated at 77 and 300 K. This work presents in-depth understandings about the temperature dependence and fundamental working mechanism of the pyro-phototronic effect on the ZnO/perovskite heterostructure and provides guidance for the design and development of corresponding optoelectronics for ultrafast photo sensing, optothermal detection, and biocompatible optoelectronic probes.

2 Results and discussion

The temperature dependence of the pyro-phototronic effect is measured in a micro-manipulation cryogenic probe system (Janis, model ST-500-2), as schematically shown in Fig. 1(a). By applying liquid nitrogen as the cryostat, the temperature of the whole system ranges from 77 to 300 K. The device structure of a self-powered ZPH PD is schematically illustrated in Fig. 1(b). The side-view scanning electron microscopy (SEM, Hitachi SU8010) image presented in Fig. 1(c1) shows that the fluorine-doped tin oxide (FTO) glass cathode is uniformly covered by the hydrothermally grown ZnO nanowire array with lengths of 500 nm and diameters of 50–70 nm (inset of Fig. 1(c2)), followed by a layer of $CH_3NH_3PbI_3$ ($MAPbI_3$) perovskite with an average thickness of 500 nm (Fig. 1(c2)) and a layer of the hole-transport material (HTM) spiro-OMeTAD with a thickness of 500–1,000 nm. Finally, a layer of Cu with a thickness of 250 nm is deposited on the top as an anode. During the measurements, ZPH PDs are attached to the surface of the cryostat with a layer of Kapton tape (30 μm thick) in between to provide stable thermal conduction and excellent electrical insulation. A 325-nm UV laser is utilized as an optical stimulus for studying the pyro-phototronic effect on the UV sensing performances of the ZPH PDs. The electric output signals are measured and collected by computer-controlled program through a general-purpose interface bus (GPIB) controller. The detailed fabrication processes of the ZPH PDs and the measurement setup are found in the Methods section.

The energy-band alignment among different layers within the ZPH PDs is depicted in Fig. 1(d). Upon UV

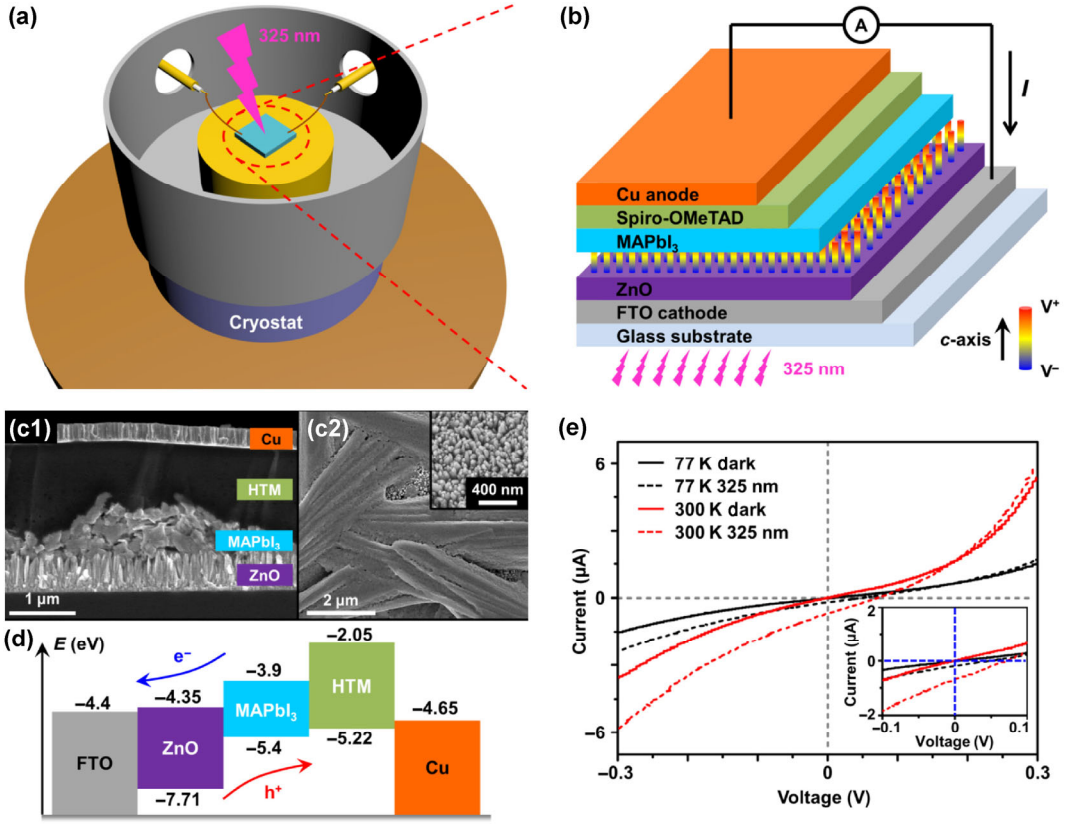

Figure 1 Structure, characterization, and operating mechanism of self-powered ZPH PDs. (a) Schematic of the experimental setup. (b) Schematic demonstration of the structure and operating mechanism of self-powered ZPH PDs. (c1) Cross-sectional SEM image of self-powered ZPH PDs, and (c2) top-view SEM image of ZnO covered by spin-coated perovskite. Inset of (c2) shows a top-view SEM image of the hydrothermally grown ZnO nanowire array. (d) Energy-band diagram of self-powered ZPH PDs. The energies are expressed in electron volts, using the electron energy in vacuum as the reference. (e) *I*–*V* characteristics of self-powered ZPH PDs in the dark and under 325-nm UV laser illumination with a light intensity of 5.10 mW·cm^{-2} at 77 and 300 K. The inset presents enlarged *I*–*V* curves indicating self-powered operations at zero bias.

illumination, electron–hole pairs are generated in the ZnO layer, with photogenerated electrons injected from the ZnO layer and collected by the FTO cathode, while the photogenerated holes in the valence band reach the Cu anode through the HTM layer. The fundamental operating mechanism of the self-powered ZPH PDs under UV illumination is illustrated in two processes: a photovoltaic process and a pyroelectric process. UV illumination-generated electrons and holes are separated at the interface, collected by electrodes, and finally recombined through the external circuit, producing the photovoltaic effect-induced current I_{photo} (Fig. S1(a), left panel, in the Electronic Supplementary Material (ESM)). This is the photovoltaic process. UV illumination also generates a fast temperature increase inside the ZnO layer to induce pyroelectric polarization potentials that are distributed across the ZnO nanowires because of their non-central symmetric crystal structures. Determined by the *c*-axis direction of the ZnO nanowires, as shown in Fig. 1(b), the positive pyroelectric polarizations are located on the Cu anode side, whereas the negative pyroelectric polarizations are present at the FTO cathode side, forming a pyro-potential field that aligns the nanowire and thus enhances the transient current with a pyroelectric effect-induced current I_{pyro} (Fig. S1(a), middle panel, in the ESM). This is the pyroelectric process. The total photocurrent of a self-powered ZPH PD upon UV illumination is therefore the sum of I_{photo} and I_{pyro}, which is the pyro-phototronic effect (Fig. S1(a), right panel, in the ESM).

The *I*–*V* characteristics of a self-powered ZPH

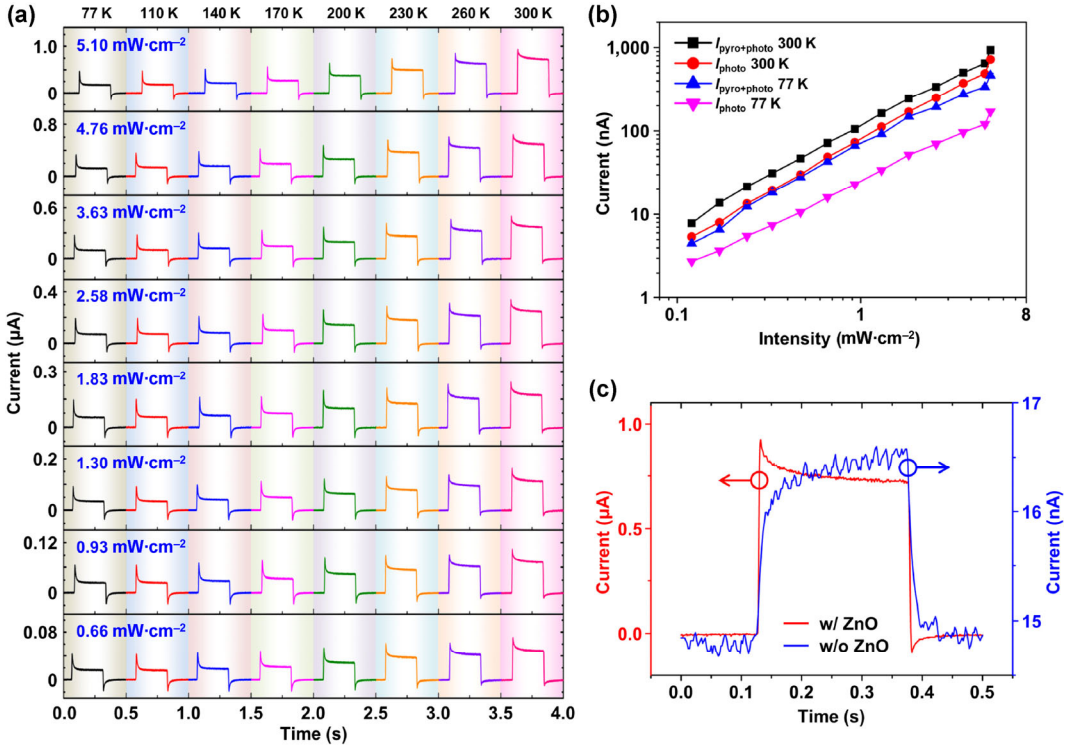

Figure 2 Current response of self-powered ZPH PDs under different temperatures and UV light intensities. (a) *I*–*t* characteristics of self-powered ZPH PDs at different temperatures ranging from 77 to 300 K under 325-nm UV laser illuminations with different light intensities from 5.10 to 0.66 mW·cm^{-2}. (b) Photocurrent responses to the pyro-phototronic and photovoltaic effect at 77 and 300 K, with zero bias voltage. (c) *I*–*t* characteristics of self-powered ZPH PDs and a device without a ZnO layer under 325-nm UV laser illumination with a light intensity of 5.10 mW·cm^{-2} at 300 K.

PD in the dark and under 325 nm UV illumination (5.10 mW·cm^{-2}) at 77 K (black lines) and 300 K (red lines) are measured and plotted in Fig. 1(e), with the inset showing the measurable photocurrents under UV illumination at zero bias: ~0.2 μA at 77 K and ~0.7 μA at 300 K. The *I*–*V* curves of PDs in the dark and under UV illumination at various temperatures ranging from 77 to 300 K are plotted in Figs. S1(b) and S1(c) (in the ESM), respectively, showing that the current decreases as the system temperature is reduced.

The current responses of the self-powered ZPH PD to temperatures under different UV illuminations are systematically investigated and summarized in Fig. 2(a) and Fig. S2 (in the ESM), by varying the UV light intensities from 5.10 to 0.12 mW·cm^{-2} at each temperature. As shown in Fig. 2(a), two-stage photocurrents are observed with a sharp current peak ($I_{pyro+photo}$) occurring at the initial stage owing to the light self-induced pyro-phototronic effect occurring upon UV illumination, followed by a steady plateau (I_{photo}) as the temperature remains unchanged and the pyroelectric polarizations disappear. The corresponding $I_{pyro+photo}$ and I_{photo} of the self-powered ZPH PDs at 77 and 300 K are extracted and plotted in Fig. 2(b) to demonstrate the enhancement of the output currents by the pyro-phototronic effect. It is straightforward that both $I_{pyro+photo}$ and I_{photo} increase monotonically with the light intensity at 77 and 300 K. Moreover, the average enhancement of the output current from I_{photo} to $I_{pyro+photo}$ at 77 K is ~155%, which is far higher than that of ~47% at 300 K. The ZnO nanowires are responsible for the pyroelectric polarizations and essential for the UV sensing performances of ZPH PDs. Control experiments are conducted under the same conditions (300 K, 5.10 mW·cm^{-2}) to verify the significance of ZnO by fabricating devices without a ZnO layer. A comparison of the current responses to the UV illuminations between devices with and without a ZnO layer is shown in Fig. 2(c). Obviously, no initial peaks are observed for the devices without

a ZnO layer, owing to the absence of the pyro-phototronic effect, and the general UV responses are far weaker with the current increasing from ~15 nA (dark) to ~16.5 nA (5.10 mW·cm^{-2}) compared with the case where the current of the ZPH PDs increases from ~1 nA (dark) to a few hundred nanoamperes at 5.10 mW·cm^{-2}. This large current on/off ratio could mainly be caused by the improved photovoltaic performance of the ZnO/perovskite heterostructure due to the elimination of a possible short circuit after the introduction of the ZnO layer. These results indicate that the ZnO layer plays a significant role in high-performance UV PDs.

The influences of the temperatures and UV light intensities on the output-current enhancement caused by the pyro-phototronic effect are evaluated by defining and calculating the parameter $R = (I_{pyro+photo} - I_{photo})/I_{photo}$, as plotted in Fig. 3. The three-dimensional (3D) plot in Fig. 3(a) shows that a larger value of R is obtained under a lower temperature and stronger UV illumination, indicating that the enhancements of the output currents due to the pyro-phototronic effect improve as the temperature decreases and the UV light intensity increases. Two two-dimensional plots obtained by extracting the projection of R versus the temperature under each UV light intensity and R versus the UV light intensity at each temperature from Fig. 3(a) are shown in Figs. 3(b) and 3(c), respectively. As clearly illustrated in Fig. 3(b), R increases monotonically as the temperature decreases at almost all light intensities, indicating that further enhancements of the output currents are caused by the pyro-phototronic effect at a lower system temperature. This is because more temperature changes are induced within the ZnO layer at a lower system temperature upon the same UV illuminations. Additionally, a lower system temperature leads to a smaller I_{photo}, which contributes to the monotonic increase of R. According to Fig. 3(c), at most temperatures (77–260 K), as the UV light intensity increases, the light self-induced temperature changes within ZnO are enhanced, leading to increases in I_{pyro} and $I_{pyro+photo}$. I_{photo} also increases with the light intensity. Thus, the parameter R initially increases, then stays steady, and finally decreases because of the increase of I_{pyro} and I_{photo} with the light intensity. At room temperature (300 K), I_{photo} increases more than $I_{pyro+photo}$ under weak UV illumination, leading to the decrease of R with increasing UV light intensity.

The temperature dependence of the output-current

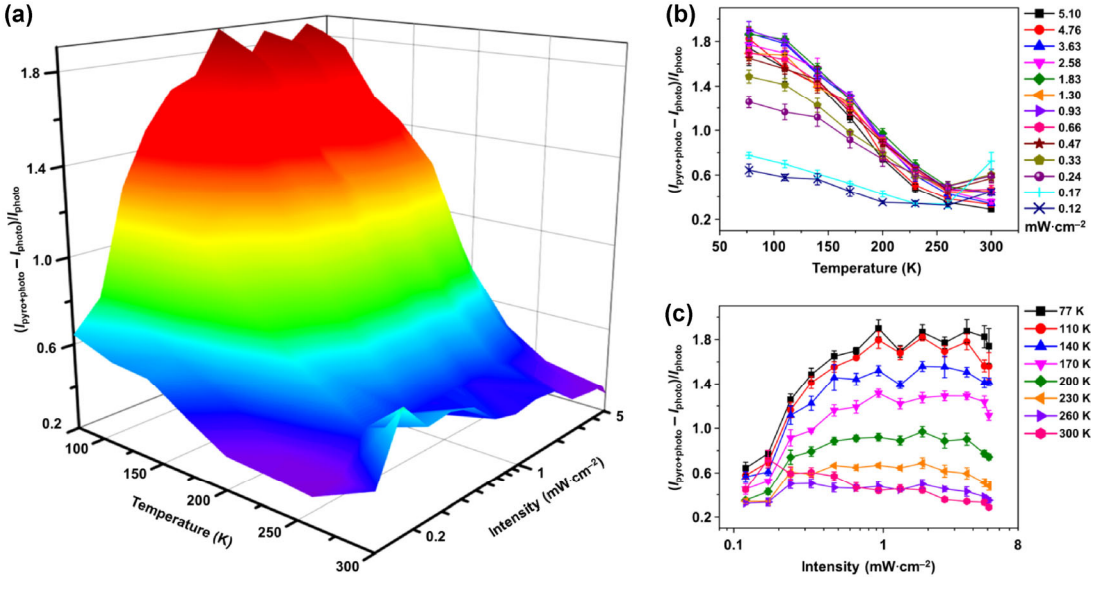

Figure 3 Temperature dependence of enhancements of output currents caused by the pyro-phototronic effect. (a) 3D surface plot depicting the output-signal enhancement caused by the pyro-phototronic effect under different temperatures and light intensities. (b) Output-signal enhancement caused by the pyro-phototronic effect under different temperatures, with the light intensity ranging from 5.10 to 0.12 mW·cm^{-2}. (c) Output-signal enhancement caused by the pyro-phototronic effect under different UV light intensities, with the temperature ranging from 77 to 300 K.

enhancement caused by the pyro-phototronic effect is determined by calculating the relative changes of R with respect to the temperature, as follows: $E = (R_T - R_{300K})/R_{300K}$ (Fig. S3 in the ESM). In most cases, the parameter E increases monotonically as the temperature decreases, with an average improvement of ~269% from 300 to 77 K for all the UV light intensities. In particular, under UV illumination of 5.10 mW·cm^{-2}, the pyro-phototronic effect-induced output-current enhancements at 77 and 300 K are 174.1% and 28.7%, respectively, showing a significant improvement of the output-current enhancement over 500% due to the pyro-phototronic effect as the temperature decreases from 300 to 77 K.

The current responses of the self-powered ZPH PDs to a typical on/off UV illumination cycle are presented in Fig. 4 to elucidate the charge-transfer processes. A general exponential function [27, 28] is applied to simulate the I–t curve, as presented in Fig. 4(a), showing a good match between the experimental and fitting results. The amount of transferred charges driven by the pyroelectric effect, Q_{pyro}, is derived by integrating the I–t curve above the reference value I_{photo} obtained from the exponential fitting. As plotted in Fig. S4 (in the ESM), Q_{pyro} increases monotonically with the UV light intensity at each system temperature. The time constant τ at the falling edge of the pyroelectric current I_{pyro} is also derived from the exponential fitting at each condition. The average value of the pyroelectric current $I_{pyro\text{-}ave} = Q_{pyro}/\tau$ is thus calculated as a parameter to quantitatively evaluate the enhancement of the UV sensing performances and to characterize the temperature dependence of the pyro-phototronic effect.

The temperature dependence of the charges transferred because of the pyroelectric effect, Q_{pyro}, is investigated under various light intensities with respect to Q_{pyro} at 300 K, as shown in Fig. 4(b) and Fig. S5 (in

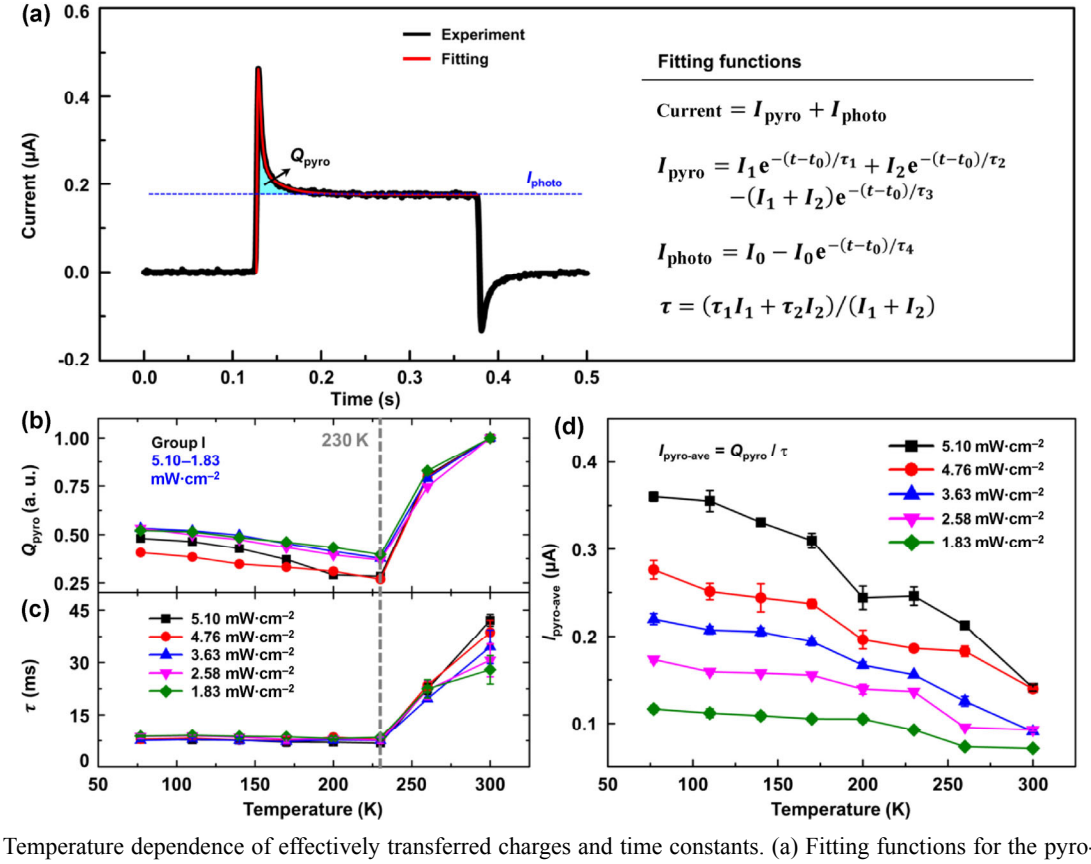

Figure 4 Temperature dependence of effectively transferred charges and time constants. (a) Fitting functions for the pyro-phototronic current $I_{pyro+photo}$ and the derivation of the transferred charges and time constants. Temperature dependence of (b) normalized transferred charge amounts, (c) time constants, and (d) averaged pyro-phototronic currents $I_{pyro\text{-}ave}$, under a UV light intensity ranging from 5.10 to 1.83 mW·cm^{-2}.

the ESM). A local minimum of the normalized Q_{pyro} is observed as the system temperature decreases from 300 to 77 K. Under a certain UV light intensity, as the system temperature decreases, the pyroelectric polarizations increase and drive the transfer of additional charges through the external circuit, as the temperature changes in ZnO are enhanced at lower background temperatures. On the other hand, the quantity and mobility of the charge carriers in a ZnO semiconductor generally decrease as the temperature decreases because more mobile charge carriers are trapped in the shallow impurity centers (i.e., the freeze-out effect) [27], which reduces the amount of transferred charges. A competition mechanism is formed between these two processes and leads to the local minimum. As shown in Fig. 4(b), as the temperature decreases from 300 to 230 K, the freeze-out effect dominates the charge-transfer process over the pyroelectric effect, leading to the decrease of Q_{pyro}. By further decreasing the temperature from 230 to 77 K, the freeze-out effect is gradually saturated, whereas the pyroelectric effect is significantly enhanced because of the low background temperature and starts to dominate, resulting in the increase of Q_{pyro}. The temperature T_0 where the minimum Q_{pyro} occurs increases with the UV light intensity because more photoexcited carriers are generated under the higher light intensity to partially screen the freeze-out effect. Consequently, with the increase of the UV light intensity, T_0 increases, from 170 K (0.24–0.12 mW·cm^{-2}) to 200 K (1.30–0.33 mW·cm^{-2}) and then to 230 K (5.10–1.83 mW·cm^{-2}).

Similar results are observed for the temperature dependence of the time constant τ at the falling edge of the pyroelectric current I_{pyro} under each UV light intensity, as shown in Fig. 4(c) and Fig. S5 (in the ESM). Overall, the time constant τ decreases to a minimum and then remains almost unchanged as the temperature decreases from 300 to 77 K, with the same T_0 that is observed for Q_{pyro} under each UV light intensity condition. Generally, the pyroelectric current I_{pyro} is proportional to the temperature-variation rate dT/dt [28]. Hence, the time constant τ corresponds to the period from the beginning to the point at which the temperature of ZnO reaches a steady state upon UV illumination. As the temperature decreases, the thermal conductivity and diffusivity of ZnO increase [29, 30], which enhances the thermal diffusion and reduces the time constant τ. The thermal dissipation of ZnO increases and prevents the temperature of ZnO from approaching the steady state. The combination of these two processes results in the observation of the minimum time constant τ, as shown in Fig. 4(c) and Figs. S5(b) and S5(d) (in the ESM).

According to the results for Q_{pyro} and τ shown in Figs. 4(b) and 4(c), respectively, it is straightforward to derive the temperature dependence of the pyro-phototronic effect by plotting the average pyroelectric current $I_{pyro\text{-}ave}$ with respect to the temperature, as shown in Fig. 4(d) and Fig. S6 (in the ESM). $I_{pyro\text{-}ave}$ increases as the temperature decreases and the UV light intensity increases. Under 5.10-mW·cm^{-2} UV illuminations, the $I_{pyro\text{-}ave}$ increases from ~0.14 μA at 300 K to ~0.36 μA at 77 K, indicating an improvement of over 100%. For all the temperatures from 77 to 300 K, $I_{pyro\text{-}ave}$ is enhanced from a few to hundreds of nanoamperes, with improvements of two orders of magnitude, by increasing the UV light intensity from 0.12 to 5.10 mW·cm^{-2}.

The bias voltage applied across the ZPH PDs also affects the enhancements of the output currents caused by the pyro-phototronic effect. The parameter $R = (I_{pyro+photo} - I_{photo})/I_{photo}$ is investigated under different bias voltages at 77 and 300 K, as shown in Fig. 5. The output-current enhancements caused by the pyro-phototronic effect are greatly reduced under high bias voltages (Fig. 5(a)) at both 77 and 300 K. Figures 5(b)–5(d) and Fig. S7 (in the ESM) show the transient current responses to UV illumination of 5.10 mW·cm^{-2} under different bias voltages ranging from 0 to 0.4 V at 77 and 300 K, clearly indicating the gradual disappearance of the pyro-phototronic effect-induced current peak $I_{pyro+photo}$ with an increasing bias voltage. At a high bias voltage, a large dark current of a few microamperes is produced, which increases the background temperature of the device, depressing the pyroelectric polarization potentials in ZnO and hence reducing the pyro-phototronic effect-related enhancements of the output currents. The peak $I_{pyro+photo}$ completely disappears as the bias voltage reaches 0.4 V at 300 K (Fig. 5(d)). At 77 K, this disappearance is observed as the bias voltage reaches 0.6 V (Fig. S8 in the ESM).

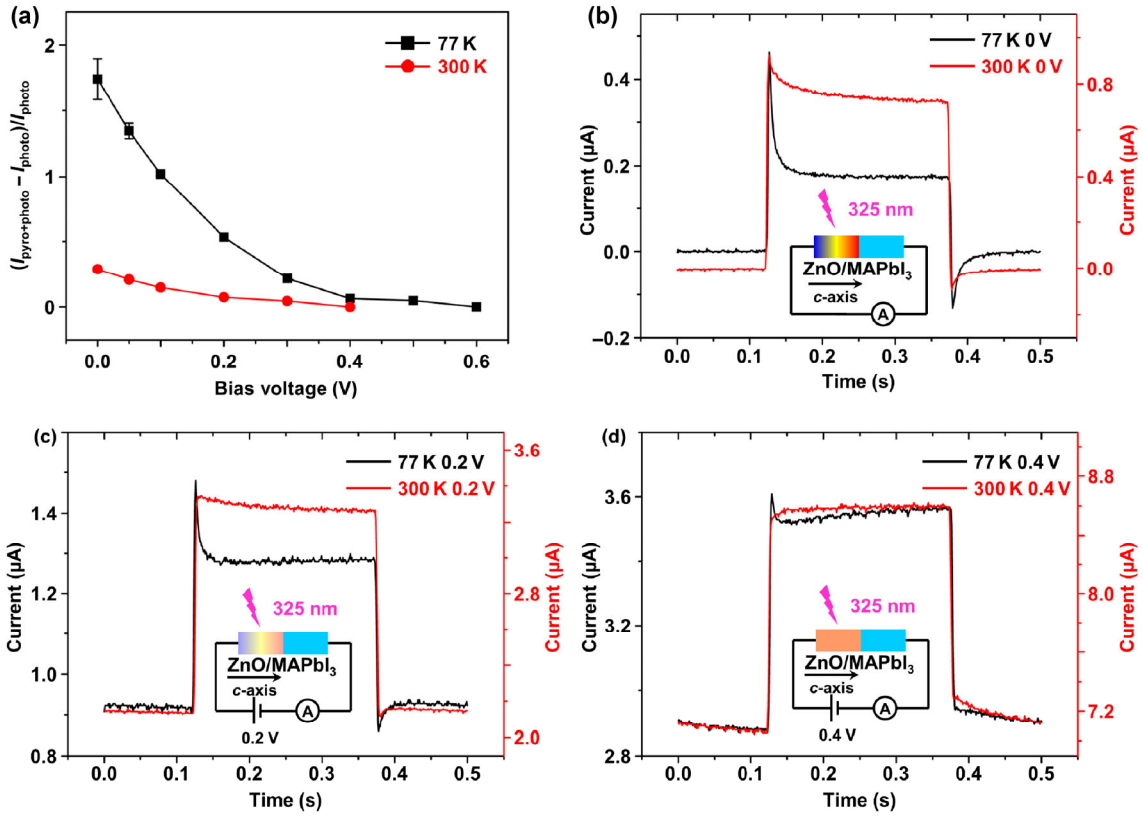

Figure 5 Effects of bias voltages on the pyro-phototronic effect in a ZnO/perovskite heterostructure. (a) Pyro-phototronic enhancement of output currents under different bias voltages at 77 and 300 K. The *I*–*t* characteristics of self-powered ZPH PDs under different bias voltages of (b) 0, (c) 0.2, and (d) 0.4 V at 77 and 300 K.

3 Conclusions

The temperature dependence of the pyro-phototronic effect-related enhancements of self-powered ZnO/perovskite heterostructured PDs is systematically investigated under various UV light intensities with the system temperature ranging from 77 to 300 K. Upon UV illumination, more temperature changes are obtained in ZnO at a lower system temperature, leading to a significant improvement of over 500% in the output-current enhancement due to the pyro-phototronic effect as the temperature decreases from 300 to 77 K. According to the exponential fittings of the current responses to UV illumination, the charges transferred through the external circuit driven by the pyroelectric polarizations are calculated and analyzed to provide insights about the working mechanism of the pyro-phototronic effect. In addition, increasing the bias voltage applied to the device effectively reduces the pyro-phototronic effect-related enhancements at both a low temperature (77 K) and room temperature (300 K). This work presents in-depth understandings about the temperature dependence and fundamental operating mechanism of the pyro-phototronic effect in ZnO/perovskite heterostructures and provides guidance for the design and development of corresponding optoelectronics for ultrafast photo sensing, optothermal detection, and biocompatible optoelectronic probes.

4 Methods

4.1 Fabrication Process of ZPH PDs

CH_3NH_3I was synthesized and purified according to a previously reported method [31]. The synthesized CH_3NH_3I powder was mixed with PbI_2 (Aldrich) at a mole ratio of 1:1 in N,N-dimethylmethanamide (DMF) at 60 ℃ for 12 h, followed by filtering twice using a 13-mm-diameter and 0.45-mm-pore polyvinylidene

difluoride syringe filter (Whatman). The derived product was used as a coating solution for the formation of $MAPbI_3$. Then, a $MAPbI_3$ perovskite DMF solution with 40 wt.% was prepared for further use. FTO glasses (Sigma-Aldrich, 13 Ω^{-2}) were ultrasonically cleaned for 5 min in acetone, distilled water, and ethanol, in sequence. Next, a 50-nm ZnO seed layer was deposited on the FTO glasses by radio-frequency magnetron sputtering at room temperature (PVD75 system, Kurt. J. Lesker Company). The coated FTO glasses were then placed into the mixed nutrient solutions (0.02 M $Zn(NO_3)_2$ and 0.02 M hexamethylenetetramine (HMTA)) for ZnO nanowire growth via a hydrothermal method in a mechanical convection oven (model Yamato DKN400, Santa Clara, CA, USA) at 85 °C for 30 min. To obtain separated ZnO nanowires, 0–5 mL of ammonium hydroxide (Sigma- Aldrich) was added per 100 mL of mixing solution. After the whole system was cooled, the product was washed with ethanol and distilled water, collected, and vacuum-dried at 100 °C for 1 h. A 40 wt.% perovskite DMF solution was spin-coated on the dried ZnO nanowire array at 4,000 rpm, and then the spiro- OMeTAD was spin-coated as a thin hole-transport layer with a spin coater (SCS 6800). Another thin layer of Cu (250 nm) was subsequently deposited as the bottom electrode. Testing wires were connected to the top and bottom electrodes using a silver paste. Finally, a thin layer of Kapton tape was employed to fix the testing wires and improve its resistance to environmental contamination and corrosion.

4.2 Optical and electrical measurements

The electric signals of the device were measured and recorded by a customized computer-controlled measurement system with a function generator (Model No. DS345, Stanford Research Systems, Inc.) and low-noise current preamplifier (Model No. SR 570, Stanford Research Systems, Inc.) in conjunction with a GPIB controller (GPIB-USB-US, NI 488.2). The optical input stimuli were provided by a He-Cd dual-color laser (wavelengths of 325 and 442 nm, Model No. KI5751I-G, Kimmon Koha Co, Ltd.). A continuously variable filter was used to control the light intensity, which was measured using a thermopile powermeter (Newport 818 P-001-12).

Acknowledgements

This research was supported by the U.S. Department of Energy, Office of Basic Energy Sciences (No. DE-FG02-07ER46394). W. B. P. would like to thank for the support from China Scholarship Council (CSC).

Electronic Supplementary Material: Supplementary material (Figs. S1–S8) is available in the online version of this article at http://dx.doi.org/10.1007/s12274-016-1240-5.

References

[1] Wang, Z. L.; Song, J. H. Piezoelectric nanogenerators based on zinc oxide nanowire arrays. *Science* **2006**, *312*, 242–246.

[2] Yang, R. S.; Qin, Y.; Dai, L. M.; Wang, Z. L. Power generation with laterally packaged piezoelectric fine wires. *Nat. Nanotechnol.* **2009**, *4*, 34–39.

[3] Wu, W. Z.; Wen, X. N.; Wang, Z. L. Taxel-addressable matrix of vertical-nanowire piezotronic transistors for active and adaptive tactile imaging. *Science* **2013**, *340*, 952–957.

[4] Ju, S.; Lee, K.; Janes, D. B.; Yoon, M.-H.; Facchetti, A.; Marks, T. J. Low operating voltage single ZnO nanowire field-effect transistors enabled by self-assembled organic gate nanodielectrics. *Nano Lett.* **2005**, *5*, 2281–2286.

[5] Wu, W. Z.; Wei, Y. G.; Wang, Z. L. Strain-gated piezotronic logic nanodevices. *Adv. Mater.* **2010**, *22*, 4711–4715.

[6] Yu, R. M.; Wu, W. Z.; Pan, C. F.; Wang, Z. N.; Ding, Y.; Wang, Z. L. Piezo-phototronic boolean logic and computation using photon and strain dual-gated nanowire transistors. *Adv. Mater.* **2015**, *27*, 940–947.

[7] Huang, M. H.; Mao, S.; Feick, H.; Yan, H. Q.; Wu, Y. Y.; Kind, H.; Weber, E.; Russo, R.; Yang, P. D. Room-temperature ultraviolet nanowire nanolasers. *Science* **2001**, *292*, 1897–1899.

[8] Pan, C. F.; Dong, L.; Zhu, G.; Niu, S. M.; Yu, R. M.; Yang, Q.; Liu, Y.; Wang, Z. L. High-resolution electroluminescent imaging of pressure distribution using a piezoelectric nanowire LED array. *Nat. Photonics* **2013**, *7*, 752–758.

[9] Kim, D. C.; Jung, B. O.; Kwon, Y. H.; Cho, H. K. Highly sensible ZnO nanowire ultraviolet photodetectors based on mechanical schottky contact. *J. Electrochem. Soc.* **2012**, *159*, K10–K14.

[10] Soci, C.; Zhang, A.; Xiang, B.; Dayeh, S. A.; Aplin, D. P. R.; Park, J.; Bao, X. Y.; Lo, Y. H.; Wang, D. ZnO nanowire UV photodetectors with high internal gain. *Nano Lett.* **2007**, *7*, 1003–1009.

[11] Wang, Z. N.; Yu, R. M.; Wen, X. N.; Liu, Y.; Pan, C. F.; Wu, W. Z.; Wang, Z. L. Optimizing performance of silicon-based p–n junction photodetectors by the piezo-phototronic effect. *ACS Nano* **2014**, *8*, 12866–12873.

[12] Özgür, Ü.; Alivov, Y. I.; Liu, C.; Teke, A.; Reshchikov, M. A.; Doğan, S.; Avrutin, V.; Cho, S. J.; Morkoç, H. A comprehensive review of ZnO materials and devices. *J. Appl. Phys.* **2005**, *98*, 041301.

[13] Jin, Y. Z.; Wang, J. P.; Sun, B. Q.; Blakesley, J. C.; Greenham, N. C. Solution-processed ultraviolet photodetectors based on colloidal ZnO nanoparticles. *Nano Lett.* **2008**, *8*, 1649–1653.

[14] Dai, J.; Xu, C. X.; Xu, X. Y.; Guo, J. Y.; Li, J. T.; Zhu, G. Y.; Lin, Y. Single ZnO microrod ultraviolet photodetector with high photocurrent gain. *ACS Appl. Mater. Interfaces* **2013**, *5*, 9344–9348.

[15] Ryu, Y. R.; Lee, T. S.; Lubguban, J. A.; White, H. W.; Park, Y. S.; Youn, C. J. ZnO devices: Photodiodes and p-type field-effect transistors. *Appl. Phys. Lett.* **2005**, *87*, 153504.

[16] Peng, W. B.; He, Y. N.; Wen, C. B.; Ma, K. Surface acoustic wave ultraviolet detector based on zinc oxide nanowire sensing layer. *Sens. Actuat. A: Phys.* **2012**, *184*, 34–40.

[17] Peng, W. B.; He, Y. N.; Zhao, X. L.; Liu, H.; Kang, X.; Wen, C. B. Study on the performance of ZnO nanomaterial-based surface acoustic wave ultraviolet detectors. *J. Micromech. Microeng.* **2013**, *23*, 125008.

[18] Ahn, S. E.; Lee, J. S.; Kim, H.; Kim, S.; Kang, B. H.; Kim, K. H.; Kim, G. T. Photoresponse of sol–gel-synthesized ZnO nanorods. *Appl. Phys. Lett.* **2004**, *84*, 5022–5024.

[19] Keem, K.; Kim, H.; Kim, G. T.; Lee, J. S.; Min, B.; Cho, K.; Sung, M. Y.; Kim, S. Photocurrent in ZnO nanowires grown from Au electrodes. *Appl. Phys. Lett.* **2004**, *84*, 4376–4378.

[20] Jeong, M. C.; Oh, B. Y.; Lee, W.; Myoung, J. M. Optoelectronic properties of three-dimensional ZnO hybrid structure. *Appl. Phys. Lett.* **2005**, *86*, 103105.

[21] Hu, Y. F.; Zhou, J.; Yeh, P. H.; Li, Z.; Wei, T. Y.; Wang, Z. L. Supersensitive, fast-response nanowire sensors by using schottky contacts. *Adv. Mater.* **2010**, *22*, 3327–3332.

[22] Cheng, G.; Wu, X. H.; Liu, B.; Li, B.; Zhang, X. T.; Du, Z. L. ZnO nanowire schottky barrier ultraviolet photodetector with high sensitivity and fast recovery speed. *Appl. Phys. Lett.* **2011**, *99*, 203105.

[23] Wang, Z. N.; Yu, R. M.; Pan, C. F.; Li, Z. L.; Yang, J.; Yi, F.; Wang, Z. L. Light-induced pyroelectric effect as an effective approach for ultrafast ultraviolet nanosensing. *Nat. Commun.* **2015**, *6*, 8401.

[24] Heiland, G.; Ibach, H. Pyroelectricity of zinc oxide. *Solid State Commun.* **1966**, *4*, 353–356.

[25] Hsiao, C. C.; Yu, S. Y. Improved response of ZnO films for pyroelectric devices. *Sensors* **2012**, *12*, 17007–17022.

[26] Hsiao, C. C.; Huang, S. W.; Chang, R. C. Temperature field analysis for ZnO thin-film pyroelectric devices with partially covered electrode. *Sens. Mater.* **2012**, *24*, 421–441.

[27] Sze, S. M.; Ng, K. K. *Physics of Semiconductor Devices*; John Wiley & Sons: New Jersey, 2007.

[28] Lubomirsky, I.; Stafsudd, O. Invited review article: Practical guide for pyroelectric measurements. *Rev. Sci. Instrum.* **2012**, *83*, 051101.

[29] Alvarez-Quintana, J.; Martínez, E.; Pérez-Tijerina, E.; Pérez-García, S. A.; Rodríguez-Viejo, J. Temperature dependent thermal conductivity of polycrystalline ZnO films. *J. Appl. Phys.* **2010**, *107*, 063713.

[30] Zhao, Y.; Yan, Y. K.; Kumar, A.; Wang, H.; Porter, W. D.; Priya, S. Thermal conductivity of self-assembled nano-structured ZnO bulk ceramics. *J. Appl. Phys.* **2012**, *112*, 034313.

[31] Im, J. H.; Lee, C. R.; Lee, J. W.; Park, S. W.; Park, N. G. 6.5% efficient perovskite quantum-dot-sensitized solar cell. *Nanoscale* **2011**, *3*, 4088–4093.